Institute of Geophysics
Polish Academy of Sciences

Routine analysis of focal mechanism - moment tensor solutions of moderate, small magnitude events in Greece: An example of the Gulf of Corinth region

Grzegorz Kwiatek (e-mail: gregus@igf.edu.pl)
Department of Seismology, Institute of Geophysics, Polish Academy of Sciences
ul. Księcia Janusza 64, 01-452 Warszawa, Poland, webite: http://wwwseis.igf.edu.pl/

Nikolaos S. Melis (e-mail: nmelis@gein.noa.gr)
Institute of Geodynamics, National Observatory of Athens
Lofos Nimfon, Thissio, GR-118 10 Athens, Greece, website: http://bbnet.gein.noa.gr

European Geosciences Union
General Assembly 2007
Vienna, Austria, 15 – 20 April 2007

Abstract

In the present study we demonstrate a routine analysis of focal mechanisms and seismic moment tensor solutions for a group of moderate/small magnitude seismic events recorded during a five year period 2000-2004 in the Gulf of Corinth region, central Greece. The waveform data used were recorded by the Hellenic National Broadband Seismic Network (HL) of the Institute of Geodynamics, National Observatory of Athens.

Seismic moment tensor inversion of the first P-wave phase amplitudes in the time domain was performed for all selected events by a software package which is routinely used in Polish copper mines and was adapted to perform with waveform data recorded in a regional network. An application of this type to regional analysis required also an extension which was achieved by using the Spectral Ray Tracer for calculation of the take-off and incidence ray path angles for a standard 1D velocity model of the Gulf of Corinth region.

As an example, a number of 43 middle-sized earthquakes with local magnitude ranging from 3.0 to 4.4 are investigated. The maximum focal depth of the analyzed events was 121km, but about 30% were very shallow, i.e. top 5km. The goal of the analysis was to demonstrate the gain of a more detail insight into the pattern and mechanism of small-moderate magnitude events in the highly seismic active area of the Gulf of Corinth.

Event ID	Date (yyyy:mm:dd)	Time (hr:mi:se)	Lat (deg)	Lon (deg)	Depth (km)	Local magn.
37	2000-08-07	12:28:55	38.40	21.85	5	3.5
39	2000-08-22	08:54:58	38.33	22.01	5	3.5
43	2000-11-15	05:37:52	38.66	22.34	32	3.6
19	2001-02-09	20:36:44	38.26	22.09	5	3.5
45	2001-03-29	00:24:09	38.16	21.99	5	3.5
04	2001-05-16	16:50:15	38.29	21.50	24	4.1
20	2001-05-21	09:56:56	38.32	21.96	5	3.6
07	2001-05-31	09:40:58	38.17	22.06	5	3.7
08	2001-05-31	23:21:59	38.06	21.96	32	3.4
03	2001-06-01	03:20:09	38.15	22.09	8	3.9
51	2001-06-01	20:19:46	38.17	22.03	5	3.7
17	2001-12-24	20:54:23	38.36	21.76	5	4.4
22	2002-01-24	03:58:20	38.07	22.82	5	3.6
53	2002-01-24	03:58:20	38.07	22.82	5	3.6
13	2002-01-27	08:43:39	38.36	22.30	19	3.8
54	2002-02-04	10:00:41	38.72	22.94	18	3.8
24	2002-02-21	18:19:21	38.36	21.76	5	3.9
25	2002-02-24	00:29:54	38.37	21.72	5	3.8
57	2002-03-23	04:50:53	38.00	22.38	87	4.1
58	2002-04-09	06:37:45	38.11	21.96	121	3.5
26	2002-07-13	18:39:39	38.11	22.12	77	3.6
05	2002-08-14	22:50:15	38.49	22.03	18	3.5
06	2002-10-21	02:30:44	38.01	22.27	23	3.0
23	2002-10-26	18:18:29	38.11	22.77	12	3.6
61	2002-12-30	19:36:13	38.53	21.60	18	3.5
62	2003-01-10	02:59:31	38.72	22.80	15	4.2
63	2003-02-03	02:17:23	38.36	21.99	15	3.5
12	2003-03-13	17:23:29	38.21	21.59	24	3.5
01	2003-04-03	16:30:06	38.38	21.96	16	3.4
64	2003-04-24	23:42:36	38.64	22.66	22	3.9
65	2003-04-28	21:30:29	38.28	22.49	19	3.5
66	2003-06-01	01:35:55	38.00	21.83	16	3.8
67	2003-06-12	23:41:37	38.12	21.68	5	4.2
21	2003-07-25	03:27:28	38.23	22.54	21	3.9
10	2003-07-29	22:42:54	38.13	22.34	21	3.8
18	2003-07-30	09:55:10	38.09	22.37	11	3.8
68	2003-07-30	09:55:10	38.09	22.37	11	3.8
73	2003-11-18	18:31:08	38.40	22.00	7	4.1
77	2004-02-17	08:52:46	38.60	21.62	12	4.0
74	2004-04-28	07:25:37	38.32	21.82	15	4.1
76	2004-08-26	08:06:54	38.61	22.19	13	4.0
78	2004-12-17	18:44:07	38.71	22.74	15	4.3
75	2004-12-18	01:25:52	38.69	22.74	17	4.0

Table 1
The list of earthquakes analysed in this study.

Seismic Network

The Hellenic National Broadband Seismic Network (code HL), operated by the National Observatory of Athens, Institute of Geodynamics during the period of our study consisted of 22 stations equipped with broadband (20-30s) three-component seismometers, mostly of Lennartz Le-3D (20s) type. A few stations operate with Guralp CMG-40T (30s) seismometers. The sample rate is 50Hz and the Geotech Instruments DR-24 digitizers are used. Figure 2 shows the distribution of the HL Network stations. For a detailed and updated description see the following website: http://bbnet.gein.noa.gr

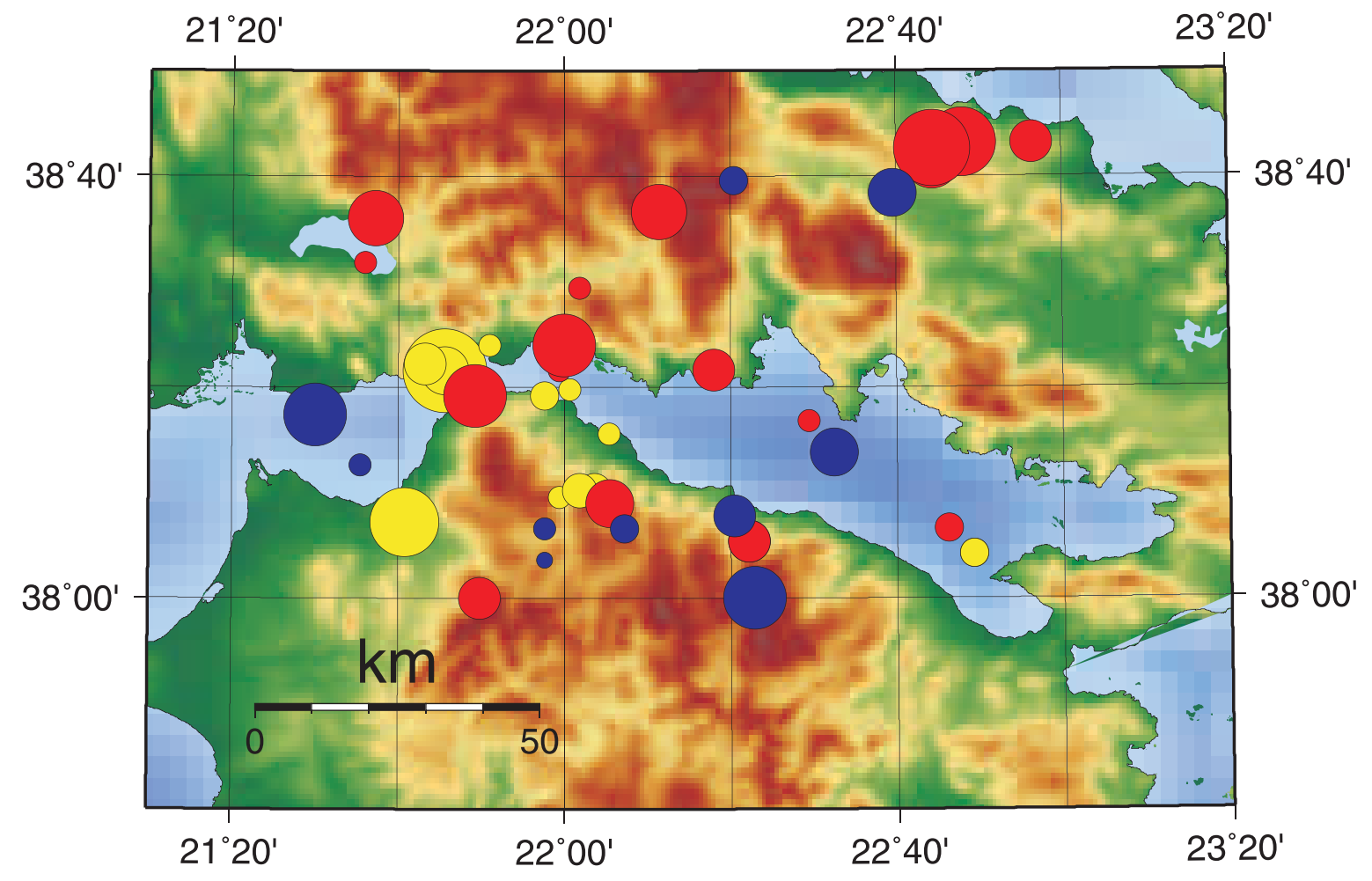

Figure 1
The distribution of analysed seismic events (stars). The size of stars depends on local magnitude (see Table 1). The **yellow**, **red** and **blue** colours denote variety of focal depth for depth<5km, 5km<depth<20km and depth> 20km, respectively.

Data

We analyzed focal mechanisms of 43 earthquakes that occurred during the time period 2000 to 2004 in the Gulf of Corinth, central Greece. Initially, we selected events from the region defined by the coordinates of a box with corners in (21°00′E, 38°00′N) and (23°00′E, 38°30′). The rectangular region is marked as a box on Figure 2, shown together with the seismic stations of the Hellenic National Broadband Seismic Network (HL). The detailed view of the study area is presented on Figure 1. The local magnitude ranging from 3.0 to 4.4. The maximum focal depth of the analyzed events was 121km, but about 30% were very shallow, i.e. top 5km.
Table 1 contains the fundamental information on selected earthquakes. The example of recorded seismograms is shown in Figure 3.

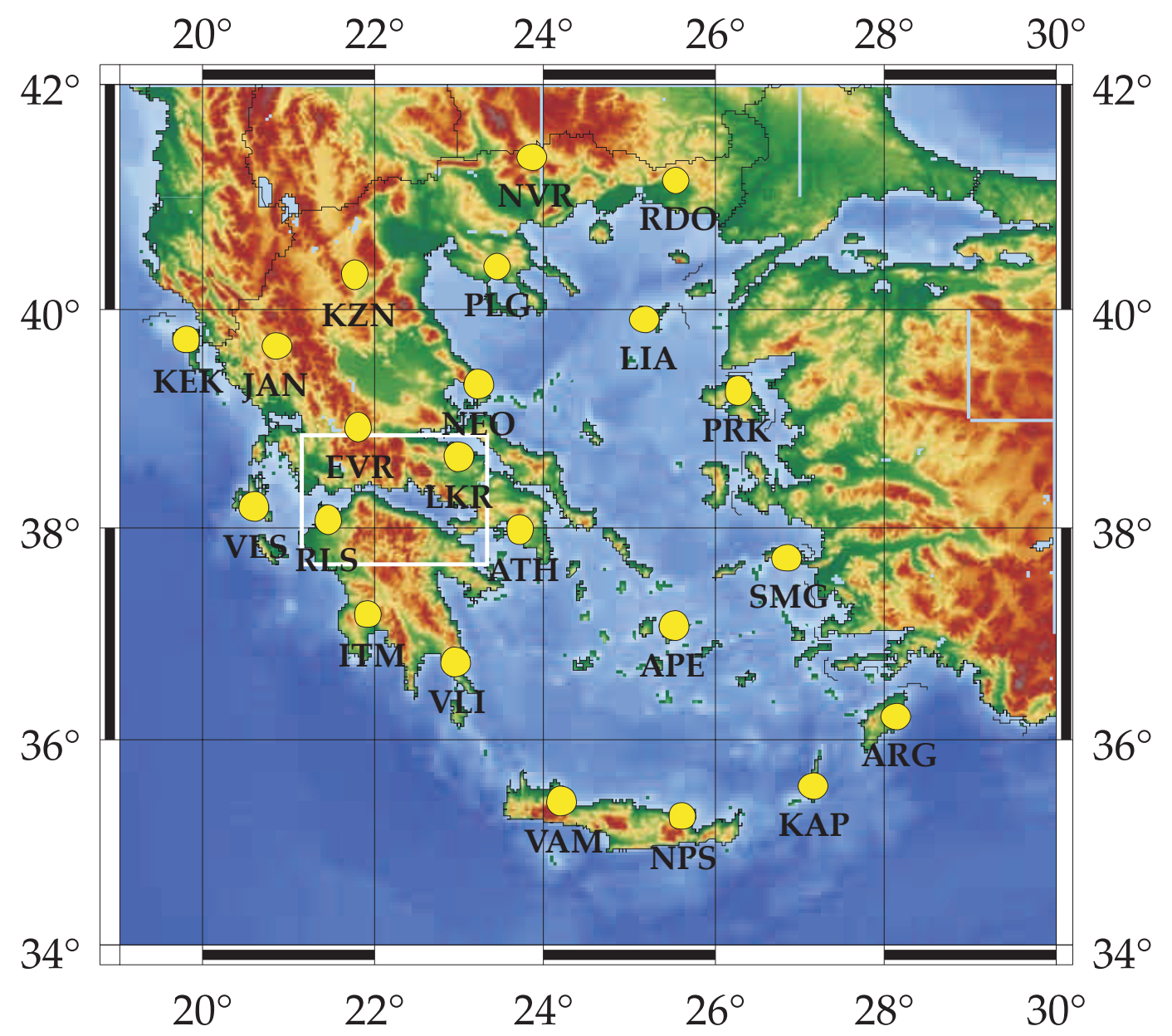

Figure 2
The surface distribution of seismic stations (yellow dots) used in this study. The white rectangle box surrounds the region of interest, which is shown in Figure 1.

Station code	Lat [deg]	Lon [deg]	Height [m]	Site name	Instrument type
APE	37.069N	25.531E	620	Apeiranthos Naxos	Le3D/ 20
ARG	36.216N	28.126E	170	Archangelos Rhodes	Le3D/ 20
ATH	37.972N	23.717E	95	Athina	STS-2
EVR	38.92N	21.81E	1050	Evritania	Le3D/ 20
ITM	37.1786N	21.9252E	400	Ithomi Messinia	Le3D/ 20
JAN	39.657N	20.851E	540	Janena	Le3D/ 20
KAP	35.55N	27.16E	530	Karpathos	CMG40T/ 30
KEK	39.71N	19.8E	280	Kerkira	Le3D/ 20
KZN	40.307N	21.771E	900	Kozani	Le3D/ 20
LIA	39.9N	25.18E	60	Limnos	CMG40T/ 30
LKR	38.65N	23E	180	Atalanti Lokrida	CMG40T/ 30
NEO	39.31N	23.22E	500	Neochori Volos	Le3D/ 20
NPS	35.263N	25.613E	370	Neapolis Crete	Le3D/ 20
NVR	41.35N	23.86E	595	Nevrokopi	CMG40T/ 30
PLG	40.374N	23.446E	580	Poligiros Chalkidiki	Le3D/ 20
PRK	39.246N	26.272E	100	Agia Paraskevi Lesvos	Le3D/ 20
RDO	41.146N	25.538E	100	Gratini Rodopi	Le3D/ 20
RLS	38.06N	21.47E	100	Riolos Achaia	Le3D/ 20
SMG	37.71N	26.84E	340	Samos	Le3D/ 20
VAM	35.407N	24.2E	225	Vamos Crete	Le3D/ 20
VLI	36.72N	22.95E	220	Velies Lakonia	Le3D/ 20
VLS	38.175N	20.59E	375	Valsamata Kefalonia	Le3D/ 20

Table 2
The detailed information on the Hellenic National Broadband Seismic Network

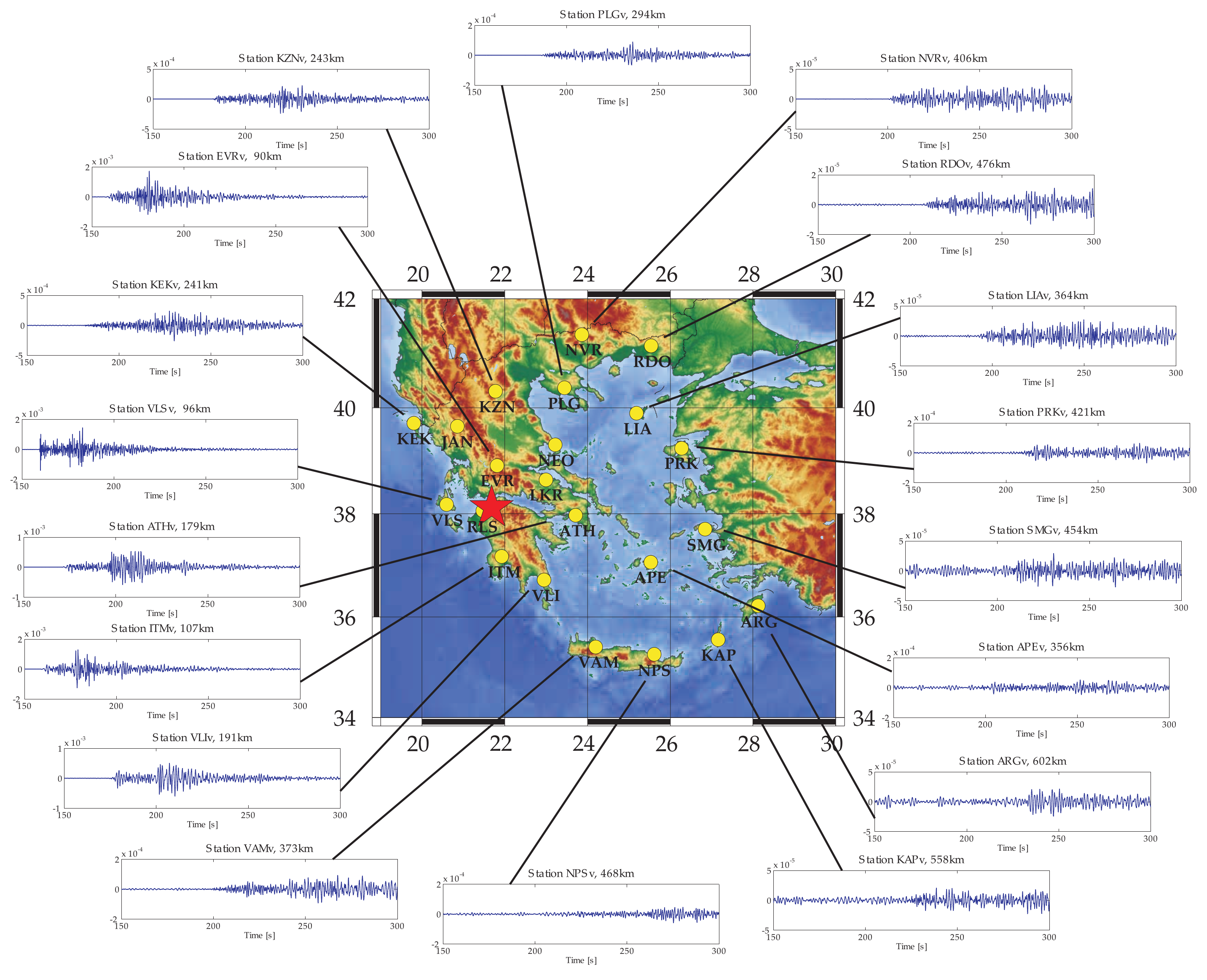

Figure 3
The example of displacement seismograms for event #67 (M_L=4.2) that occured in 2003-06-12 (red star), recorded by the Hellenic National Broadband Seismic Network. Seismograms are not scaled to the same maximum amplitude of displacement.

Moment tensor inversion

The method of inversion of first P-wave amplitudes was used to calculate the moment tensor solution based on the work of Fitch et al. (1980). Only radial component of the P-wave first arrival were taken into account. The recorded displacement of the P-wave phase is:

$$\mathbf{U}^P(x,t) = \frac{1}{4\pi\rho\alpha^3 r}\left(\overline{\gamma}\mathbf{M}\dot{S}\left(t-\frac{r}{\alpha}\right)\overline{\gamma}\right)\bar{l}$$

where ρ is the average density, **r** is a source-receiver distance, α is a P-wave average velocity and **M** is a seismic moment tensor, l is an angle of incidence and γ is a takeoff angle. The calculation of angle of incidence, takeoff angle, distance along the ray-path and average travel time were performed using Spectral Ray Tracer (see next section). We assumed a classical Source Time Function for Haskell's source model. The following, classical & linear matrix equation was considered:

$$\mathbf{GM} = \mathbf{U}^P$$

where G is a N*6 matrix (N is a number of recorded vertical amplitudes of the, for example, first P-wave velocity pulse). Matrix G describes Green's functions for the corresponding moment tensor elements, U is a vector of recorded displacements and M is a vector containing 6 independent components of the SMT in the following form:

$$\mathbf{M} = [M_{11}, M_{12}, M_{13}, M_{22}, M_{23}, M_{33}]$$

We used a robust L1 norm and an iterative procedure to solve equation (2). The full moment tensor, as well as the trace-null (trace(M)=0) and double-couple (det(M)=0 and trace(M)=0) solutions were calculated using Lagrange multipliers method.

Spectral Ray-Tracer

The spectral ray tracer (SRT) (Dębski, Ando, 2004) is a two-point ray-tracing algorithm based on the parameterization of ray paths by a series of Chebyshev polynomials. This pseudo-spectral approximation of sought ray paths allows to reach a very high accuracy of travel time calculations in 3D geological medium. In this study, we used only a 1D velocity model for the Corinth Gulf area (Figure 4).
The key point of the SRT is the representation of the sough ray path by a finite sum of Chebyshev polynomials. The optimization task, namely: finding the shortest travel time path according to Fermata's principle, is the task of searching for the scaling coefficients for which travel time reaches the global minimum, which can be solved using any suitable optimization algorithm. However, due to the nonlinearity of the problem, the Adaptive Simulated Annealing (ASA) algorithm was used. For each earthquake depth and epicentral distance, the algorithm calculated the shortest ray path from the source to the receiver, the angle of incidence, takeoff angle and average P-wave velocity.

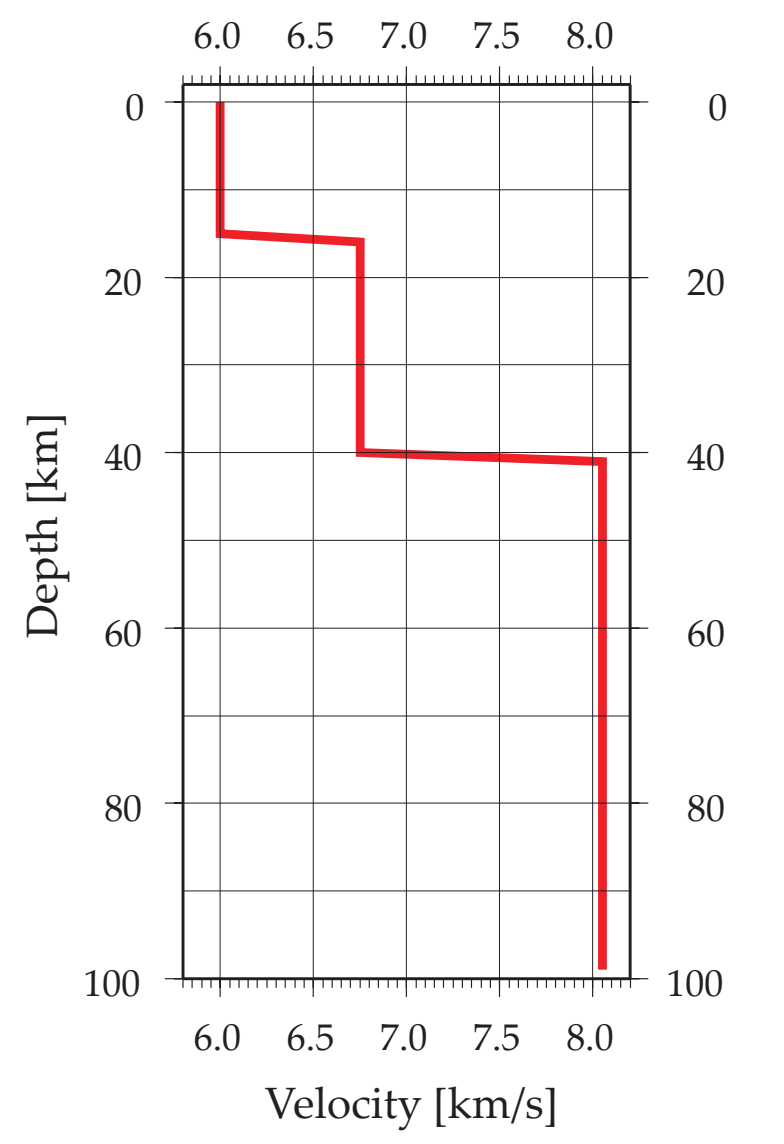

Figure 4
1D velocity model for central Greece used in this study.

Processing & Results

At the beginning, the correction for the instrument response was applied, according to either Lennartz, Guralp or STS-2 seismometer. Then, the radial component was extracted from all analyzed seismograms. Weak, 0.5 - 15Hz bandpass Butterworth filter was applied to the selected seismograms, in order to clarify the onset of the first P-wave phase. The location of events was calculated with HYPO.

We carefully picked the first P-wave amplitude. In most cases, as it was expected, we were able to mark accurately rather for a short-distant stations, ranging from 200 up to 250km (mostly from ATH, EVR, RLS, ITM, VLI, VLS, NEO and LKR). The coverage of the focal sphere was sufficient.

For some initially selected earthquakes with smaller magnitude we were not able to select the minimum number of first P-wave pulses (eight) to perform the moment tensor inversion. Problems were caused mainly due to the poor signal-to-noise ratio and the similarity between the noise and signal frequency characteristics. Hence only 43 events were finally processed for moment tensor solution.

The inversion problem was solved using L1 and (to compare) L2 norm and a special software used in Polish copper ore mines (for details see: http://www.igf.edu.pl/~gregus/foci) The moment tensor inversion was calculated with a typical constrain imposed on the shape of moment tensor matrix in order to obtain the double-couple solution. However we were able to calculate a trace-null or full solution as well.
The final set of double-couple solutions is shown in Figure 5.

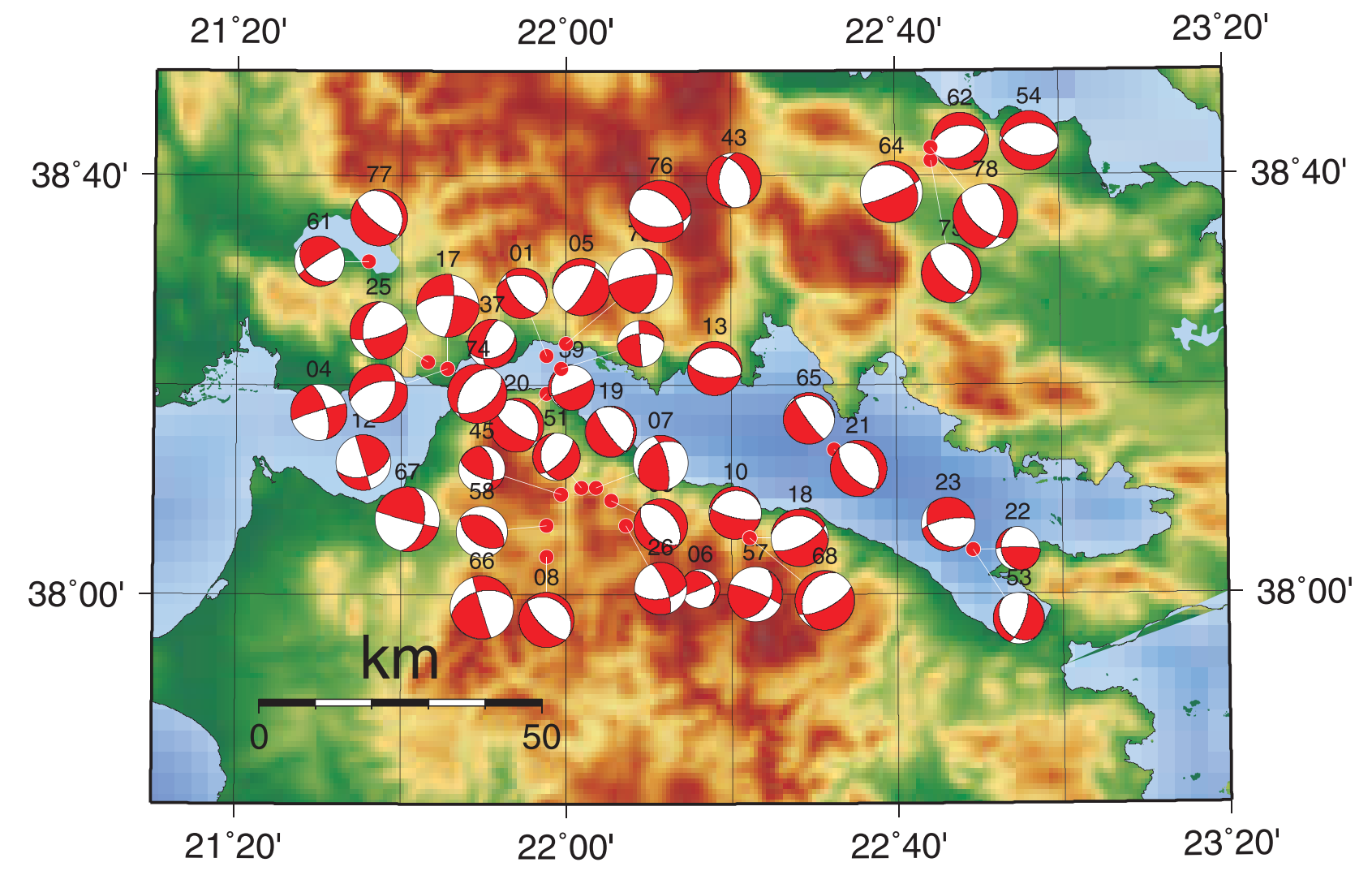

Figure 5
The surface distribution of focal mechanisms for constrained, double-couple seismic moment tensors. The equal-area, lower-hemisphere projection was used. The detailed description of focal mechanisms is shown in Table 3.

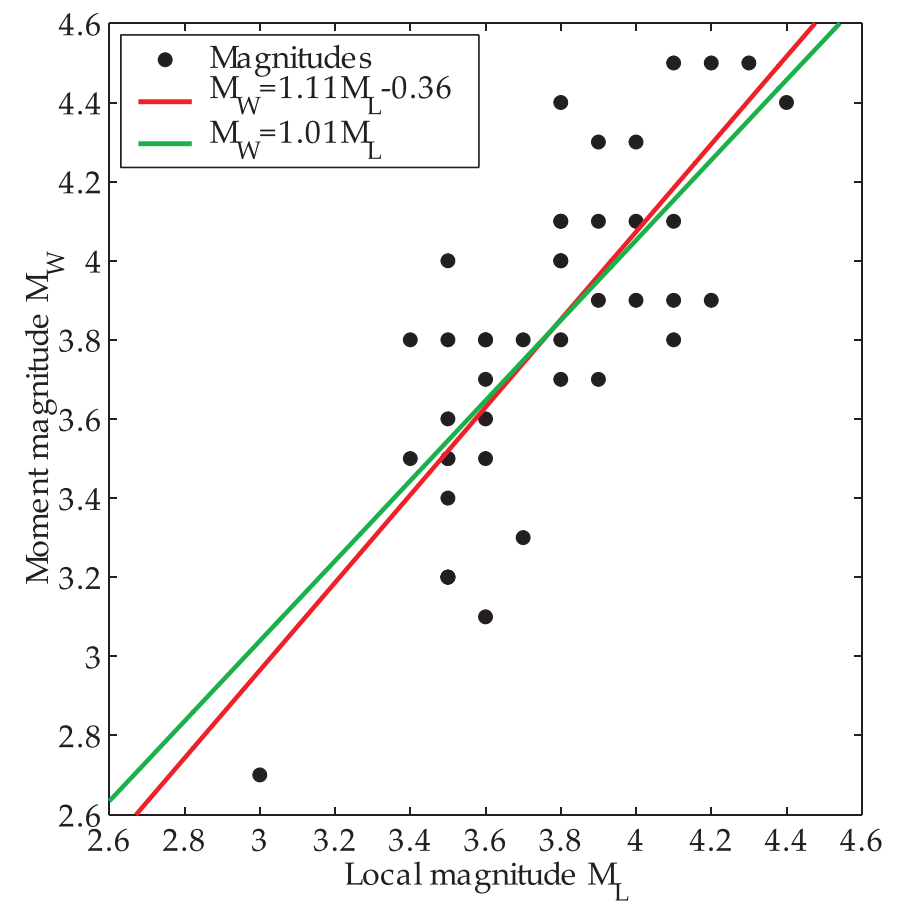

Figure 6
The dependence between local magnitude M_L and moment magnitude M_W, estimated from seismic moment according to the standard Hanks&Kanamori relationship.

Conclusions

In the present study we demonstrate a methodology for producing seismic moment tensor solutions. This was successfully applied to 43 from over 70 seismic events selected from the area of the Gulf of Corinth and recorded by the Hellenic National Broadband Seismic Network. The moment tensor inversion was performed using an adapted for the present study software package that is routinely used in Polish copper ore mines. Additionaly a spectral ray tracer was used (Dębski, Ando, 2004). Good constraint is shown for these 43 events since minimum 8 first P-wave are marked correctly and the signal-to-noise ratio is sufficiently high for the moment tensor inversion.

	Fault A			Fault B							
Event ID	Strike [deg]	Dip [deg]	Rake [deg]	Strike [deg]	Dip [deg]	Rake [deg]	Fault Type	M_0 [N · m]	M_w	ΔM	M_0^{err} [N · m]
01	141	65	-72	285	30	-108	N	$1,93\times10^{14}$	3,5	0,1	$9,34\times10^{12}$
03	133	48	-85	320	42	-95	N	$3,97\times10^{14}$	3,7	-0,2	$1,57\times10^{13}$
04	253	86	-22	345	68	-158	S	$7,48\times10^{14}$	3,9	-0,2	$4,23\times10^{13}$
05	31	76	-70	267	25	-110	N	$8,66\times10^{14}$	4	0,5	$6,08\times10^{13}$
06	67	87	58	332	32	122	R	$1,26\times10^{13}$	2,7	-0,3	$3,86\times10^{12}$
07	345	71	59	227	35	121	R	$5,51\times10^{14}$	3,8	0,1	$4,06\times10^{13}$
08	136	68	-86	306	22	-94	N	$5,39\times10^{14}$	3,8	0,4	$1,45\times10^{13}$
10	103	75	-81	253	17	-99	N	$3,01\times10^{14}$	3,7	-0,1	$5,68\times10^{13}$
12	343	90	-42	73	48	-138	S	$5,89\times10^{14}$	3,8	0,3	$4,03\times10^{13}$
13	102	65	-86	276	25	-94	N	$4,38\times10^{14}$	3,8	0	$1,36\times10^{13}$
17	6	76	-28	268	63	-152	S	$3,41\times10^{15}$	4,4	0	$1,81\times10^{14}$
18	63	69	-76	277	25	-104	N	$9,21\times10^{14}$	4	0,2	$5,22\times10^{13}$
19	144	78	-88	343	12	-92	N	$2,03\times10^{14}$	3,5	0	$7,26\times10^{12}$
20	126	69	-78	336	24	-102	N	$4,17\times10^{14}$	3,7	0,1	$2,09\times10^{13}$
21	137	58	-80	334	33	-100	N	$7,68\times10^{14}$	3,9	0	$1,07\times10^{14}$
22	271	83	65	165	26	115	R	$4,54\times10^{13}$	3,1	-0,5	$7,15\times10^{12}$
23	260	74	-65	140	29	-115	N	$4,22\times10^{14}$	3,8	0,2	$2,64\times10^{13}$
24	255	59	-55	21	46	-125	N	$1,26\times10^{15}$	4,1	0,2	$7,15\times10^{13}$
25	74	73	-49	183	44	-131	N	$9,52\times10^{14}$	4	0,2	$8,72\times10^{13}$
26	339	72	-35	81	57	-145	S	$2,78\times10^{14}$	3,6	0	$7,37\times10^{13}$
37	194	63	-57	69	42	-123	N	$1,15\times10^{14}$	3,4	-0,1	$4,80\times10^{12}$
39	68	84	-78	186	13	-102	N	$6,02\times10^{13}$	3,2	-0,3	$1,06\times10^{13}$
43	330	50	-66	185	45	-114	N	$5,03\times10^{14}$	3,8	0,2	$2,52\times10^{13}$
45	112	61	47	354	50	133	R	$6,79\times10^{13}$	3,2	-0,3	$2,44\times10^{13}$
51	45	66	-64	175	35	-116	N	$8,87\times10^{13}$	3,3	-0,4	$7,27\times10^{12}$
53	21	72	-65	145	29	-115	N	$2,00\times10^{14}$	3,5	-0,1	$7,09\times10^{12}$
54	104	51	-76	262	41	-104	N	$1,44\times10^{15}$	4,1	0,3	$8,02\times10^{13}$
57	292	82	46	30	45	134	S	$4,78\times10^{14}$	3,8	-0,3	$2,88\times10^{13}$
58	123	48	90	301	42	90	R	$2,01\times10^{14}$	3,5	0	$1,03\times10^{13}$
61	236	83	-56	136	35	-124	N	$1,62\times10^{14}$	3,5	0	$1,21\times10^{13}$
62	62	47	-78	260	45	-102	N	$8,35\times10^{14}$	3,9	-0,3	$1,75\times10^{13}$
63	175	89	-35	266	55	-145	S	$6,88\times10^{13}$	3,2	-0,3	$6,58\times10^{12}$
64	67	82	-68	318	23	-112	N	$2,59\times10^{15}$	4,3	0,4	$2,36\times10^{14}$
65	145	83	-80	269	13	-100	N	$2,28\times10^{14}$	3,6	0,1	$1,99\times10^{13}$
66	163	88	-43	255	47	-137	S	$3,53\times10^{15}$	4,4	0,6	$1,69\times10^{14}$
67	105	87	43	12	47	137	S	$5,02\times10^{15}$	4,5	0,3	$6,95\times10^{14}$
68	62	69	-73	203	27	-107	N	$1,47\times10^{15}$	4,1	0,3	$1,21\times10^{14}$
73	261	77	44	3	47	136	S	$5,02\times10^{15}$	4,5	0,4	$1,60\times10^{14}$
74	54	48	-76	213	44	-104	N	$1,43\times10^{15}$	4,1	0	$1,24\times10^{14}$
75	135	67	-72	355	29	-108	N	$1,46\times10^{15}$	4,1	0,1	$8,15\times10^{13}$
76	313	49	-61	93	48	-119	N	$2,84\times10^{15}$	4,3	0,3	$1,22\times10^{14}$
77	129	72	-80	339	21	-100	N	$7,98\times10^{14}$	3,9	-0,1	$3,74\times10^{13}$
78	133	59	-58	3	43	-122	N	$4,80\times10^{15}$	4,5	0,2	$3,60\times10^{14}$

Table 3
This table shows the result of moment tensor inversion under constraints for a double-couple solution. The fault type - (N)ormal, (S)trike slip or (R)everse is shown in 8th column. The moment magnitude (9th column) was calculated according to standard Hanks&Kanamori relationship. The difference between moment magnitude and local magnitude is shown in 10th column. The maximum error is the highest value of standard deviation from all six independent moment tensor components (taken from diagonal elements of covariance matrix for L2 solution)

Acknowledgements

This paper was supported by the NATO Collaborative Grant no. EST-CLG-979849.

Selected Bibliography

Fitch, T.J.; McCowan, D.W. & Shields, M.W. (1980) Estimation of seismic moment tensor from teleseismic body wave data with application to intraplate and mantle earthquakes, J. Geophys. Res., 85, 3817-382
Dębski, W. & Ando, M. (2004) Spectral Ray Tracer: A class of accurate two-point ray tracers, Acta Geophys. Pol. 52, pp. 1-14